Steady-state cellular growth during directional solidification

David A. Kessler
Department of Physics, University of Michigan, Ann Arbor, Michigan 48109

Herbert Levine
Department of Physics and Institute for Nonlinear Science, University of California, La Jolla, California 92093
(Received 10 March 1988)

We study cellular structures moving at constant velocity, in a symmetric model of directional solidification. This is done by employing Newton's method to solve a discretized version of the integro-differential equation for the solid-liquid boundary. Our results indicate that there is a continuous band of allowed wavelengths and that there is a generic fold in the solution diagram. This fold provides a maximum allowed wavelength for any given velocity. Also, we argue that the mechanism of microscopic solvability serves to fix the tip shape at fixed wavelength. The implications of our results for wavelength and shape selection are briefly discussed.

I. INTRODUCTION

Solidification patterns have presented many challenges to our understanding of nonequilibrium dissipative systems.[1] One issue studied extensively to date concerns velocity selection in free dendritic growth.[2] The answer turned out to involve a subtle solvability mechanism which fixes the tip structure for given undercooling. This selection mechanism has also been found to operate in related pattern-forming systems.[3]

A different issue is that of wavelength selection during directional solidification.[1] It is well known that a solidifying alloy may form a parallel array of cellular shapes (see Fig. 1) which upon increased pulling speed destablize to form parallel dendrites. In the dendrite limit, the tip region is again controlled by solvability mechanism for free growth; that is, the neighboring dendrites do not appear to be of much importance.[4] This is of course not true for cells. In both cases, however, the wavelength of the structure is a second length associated with the overall pattern.

The first studies[5] of periodic cellular patterns were performed using weakly nonlinear methods valid near the onset of Mullins-Sekerka[6] instability of the planar interface. The basic picture that emerged was that the transition could be either supercritical or subcritical (depending on parameters), that a band of allowed wavelengths exists, and that an abrupt $\lambda \rightarrow \lambda/2$ transition might occur. These calculations were extended by the work of Ungar and Brown[7] (see also McFadden and Coriell[8]) to larger velocities by means of a finite-element analysis of the diffusion equations governing the growth.[9] These results provided evidence that at least for velocities not too far above threshold, a continuous band of solutions was possible.

More recently, attention has focused on infinite cells in the one-sided limit. That is, if we completely neglect diffusion in the solid, it is possible to find cell shapes in which the liquid phase extends all the way to $y = -\infty$ (see Fig. 2 for our coordinate system). The possibility that this limiting system might exhibit sharp wavelength selection was put forth by Karma.[10] Later work by Dombre and Hakim[11] and Ben-Amar and Moussallam,[12] however, showed that this initial conclusion was incorrect; a band exists even for infinite cells. None of these papers addressed the connection between deep but finite cells and the strictly infinite case.

In this paper we return to the consideration of finite depth cells, albeit with a different and possibly more powerful calculational scheme. In particular, it has become clear that the best way of studying steady-state solidification problems is by reexpressing the field equations and boundary conditions with a single integro-differential equation for the interface. This equation is then discretized and the resulting system of coupled nonlinear ordinary differential equations solved by Newton iteration. This approach allows us to construct highly accurate interface shapes far above the small amplitude region. Although we do not attempt this in this paper, in principle this method allows for the quantitative prediction of the full range of steady-state solutions for fully realistic models of thin-film alloy solidification, at fixed velocity, thermal gradient, and thermodynamic parameters.

The major purpose of this paper is to study the generic behavior of cellular structures. Because of this, we will employ some simple approximations and focus mostly on the limit of equal chemical diffusion constants in the solid and liquid. As we will discuss, a comparison of our near-threshold results with the analogous ones of Ungar and Brown for a more realistic system demonstrates that the generic structure is independent of many of the fine details. In a later publication, we will deal with a fully accurate system of equations in an attempt to make quantitative comparisons to the experiments.

The outline of this work is as follows. In Sec. II we review the basic equations of directional solidification and the integro-differential formalism. We also comment on

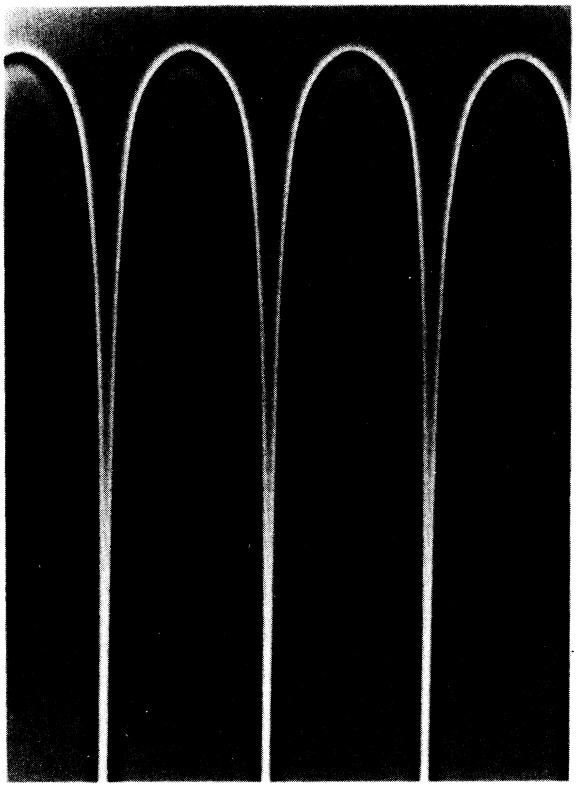

FIG. 1. Typical cellular structure seen in thin-film directional solidification of pivalic acid (see Ref. 17) (courtesy A. Libchaber).

the singular nature of the one-sided limit. In Sec. III, we specialize to a quasisymmetric model and describe our computational scheme. Section IV is devoted to results close to the ones of the Mullins-Sekerka instability, where we find agreement with both the analytical studies and the previous work of Ungar and Brown. Section V discusses behavior far above the aforementioned threshold. We discuss the tip selection problem at fixed wavelength, especially with regard to the limiting form of this issue for small surface tension. This allows us to connect our findings with the aforementioned work on infinite cellular shapes. Also, we demonstrate the existence of a maximum allowed value of the wavelength λ due to a fold appearing in the steady-state band.

This last behavior is directly connected to the $\lambda \rightarrow \lambda/2$ transition noted by Ungar and Brown. Similar behavior has been found in a study[13] of periodic patterns in Taylor-Couette systems, and can be traced to O(2) symmetry (translations and reflections) of the bifurcation problem around the planar steady state. We comment briefly on the possible relevance of this behavior for the issue of wavelength selection. Section VI summarizes our findings and describes calculations currently in progress.

II. REVIEW OF DIRECTIONAL SOLIDIFICATION

Directional solidification refers to a process whereby an alloy is solidified in the presence of an externally imposed temperature gradient. This gradient allows for the imposition of a fixed average velocity for the solid-liquid interface, under the usual assumption of equal thermal diffusivities for the different phases. The only dynamical fields are the concentrations of the alloy components. For a binary alloy, we are left with a single independent variable, with boundary conditions to be satisfied at the moving interface.

We assume that the alloy is characterized by the phase diagram of Fig. 3. The concentration obeys the diffusion equation

$$D_L \nabla^2 c = \frac{\partial c}{\partial t} \quad \text{inside the liquid ,}$$
$$D_S \nabla^2 c = \frac{\partial c}{\partial t} \quad \text{inside the solid .} \tag{1}$$

The concentration far in front of the interface approaches c_∞ which is fixed for a given process. At the interface, local thermodynamic equilibrium requires that the temperature be the same on both the liquid and solid sides. Using the phase diagram given in Fig. 3, the dependence of interface temperature on concentration in the two phases is found to be

$$T_S = \tilde{T}_M - c_S m_S ,$$
$$T_L = \tilde{T}_M - c_L m_L ,$$

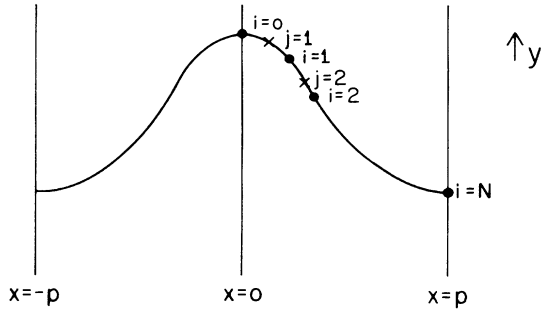

FIG. 2. Coordinate system for our analysis of cellular shapes.

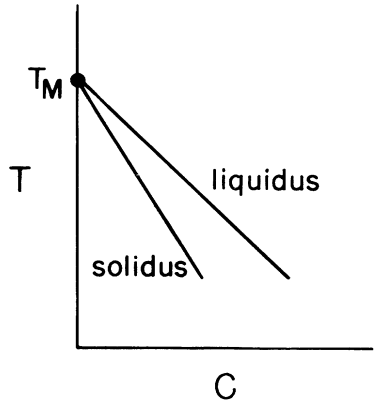

FIG. 3. Phase diagram for a binary alloy.

where m_S and m_L refer, respectively, to the slopes $\partial T/\partial c$ in the liquid and solid and phases, and c_i to the concentration on the respective sides of the interface. $\tilde{T}_M$ is the melting temperature for the pure material ($c=0$).

As is well known there is Gibbs-Thomson shift in this temperature due to curvature; $\tilde{T}_M = T_M[1-d_0(\theta)\kappa]$, where the capillary length $d_0=\sigma/L$ for surface energy σ and latent heat L can depend on the angle θ between the interface normal $\hat{\mathbf{n}}$ and the crystal axes. For fourfold crystals, we will always take

$$d_0(\theta)=d_0(1-\epsilon\cos 4\theta) \ . \tag{2}$$

Combining these results, we derive the concentration gap (sometimes called the tie line)

$$c_L-c_S=\{T_M[1-d_0(\theta)\kappa]-T_{\rm int}\}(m_S-m_L) \ , \tag{3}$$

where $T_{\rm int}$ is the actual temperature at the interface. Finally, conservation of matter requires that

$$-v_n(c_L-c_S)=D_L(\hat{\mathbf{n}}\cdot\nabla c)_L-D_S(\hat{\mathbf{n}}\cdot\nabla c)_S \ , \tag{4}$$

where v_n is the normal velocity of the moving solid-liquid interface.

To put the equations in final form, we recall that the temperature is imposed externally as

$$T(y)=T_M+Gy \ ,$$

which corresponds to the choice $y=0$ at $T=T_M$. Let us scale c by c_∞ and introduce the two lengths

$$\tilde{d}_0=d_0\frac{T_M}{m_L c_\infty} \ , \tag{5a}$$

$$\tilde{l}_T=\frac{m_L c_\infty}{G} \ , \tag{5b}$$

and set $k=m_L/m_S$. The above system of equations becomes

$$c_L=\frac{c_S}{k}=\frac{-y}{\tilde{l}_T}-\tilde{d}_0(\theta)\kappa \ ,$$

$$(D_L\hat{\mathbf{n}}\cdot\nabla_c)_L-(D_S\hat{\mathbf{n}}\cdot\nabla c)_S=-v_n(1-k)c_L \ .$$

We specialize to the case of an interface moving with a constant velocity denoted by v and transform our equations to a moving frame of reference in which the interface is stationary. Recall that we are interested in patterns which are periodic with spatial period λ. It is convenient to define dimensionless variables by measuring all lengths in units of the diffusion length $v/2D_L$. We can define a Peclet number corresponding to the ratio of a half wavelength to the diffusion length, $p=v\lambda/4D_L$. In our units, p is exactly one half wavelength. The final form of the equations is then

$$\nabla^2 c+2\frac{\partial c}{\partial y}=0 \quad \text{for the liquid} \ , \tag{6a}$$

$$\alpha\nabla^2 c+2\frac{\partial c}{\partial y}=0 \quad \text{for the solid} \ , \tag{6b}$$

$$(\hat{\mathbf{n}}\cdot\nabla c)_L-\alpha(\hat{\mathbf{n}}\cdot\nabla c)_S=-2(1-k)c_L\hat{n}_y \ , \tag{6c}$$

$$c_L=\frac{c_S}{k}=\frac{-y}{\xi}-\gamma\kappa \ , \tag{6d}$$

where $\gamma=v\tilde{d}_0/2D_L$ and $\xi=v\tilde{l}_T/2D_L$ and $\alpha=D_S/D_L$.

We can derive the integro-differential equation from the above system as follows. Let c_1 be a field equal to c everywhere in the liquid and zero in the solid. Similarly, let c_2 equal c everywhere in the solid and be equal to zero in the liquid. From Eqs. (6) and the boundary condition $c\to 1$ at ∞, we can write

$$c_1=1+\int c_L\hat{\mathbf{n}}'\cdot\nabla' G_L-\int G_L\phi_1 \ , \tag{7a}$$

$$c_2=\int c_S\alpha\hat{\mathbf{n}}'\cdot\nabla' G_S-\int G_S\phi_2 \ , \tag{7b}$$

where the Green's functions for the steady-state diffusion equation are

$$G_L=\frac{1}{4p}e^{-(y-y'+|y-y'|)}+\frac{1}{2p}\sum_{n=1}^{\infty}\frac{\cos\left[\frac{n\pi(x-x')}{p}\right]\exp(-\{y-y'+|y-y'|[1+(n\pi/p)^2]^{1/2}\})}{[1+(n\pi/p)^2]^{1/2}} \ , \tag{8a}$$

$$G_S=\frac{1}{4p}e^{-(y-y'+|y-y'|)/\alpha}+\frac{1}{2p}\sum_{n=1}^{\infty}\frac{\cos\left[\frac{n\pi(x-x')}{p}\right]\exp(-\{(y-y')/\alpha+|y-y'|[1/\alpha^2+(n\pi/p)^2]^{1/2}\})}{[1/\alpha^2+(n\pi/p)^2]^{1/2}} \ . \tag{8b}$$

From the above equation, we can derive the final interface equation by imposing the boundary condition (6c) on the gradient of the concentration field. Using the easily derived results

$$\hat{\mathbf{n}}\cdot\nabla c_L=\hat{\mathbf{n}}\cdot\nabla c_1=\phi_1-2\hat{n}_y c_L \ ,$$

$$-\alpha\hat{\mathbf{n}}\cdot\nabla c_S=-\alpha\hat{\mathbf{n}}\cdot\nabla c_2=-\phi_2+2\hat{n}_y c_S \ ,$$

Eq. (6c) reduces to $\phi_1=\phi_2\equiv\phi$. Evaluating the general expressions on the solid side of the interface yields

$$0=1+\int c_L\hat{\mathbf{n}}'\cdot\nabla' G_L-\int\phi G_L \ , \tag{9a}$$

$$c_S=-\int\alpha c_S\hat{\mathbf{n}}'\cdot\nabla' G_S \ . \tag{9b}$$

These equations, coupled with the explicit expressions for c_L and c_S given above in (6d), serve to self-consistently determine both the interface and the function ϕ.

There are two limits for which the above equations simplify. First, let us take $\alpha=1$. Then, adding the two equations above, we obtain the single requirement

$$c_S=\int (c_L-c_S)\hat{\mathbf{n}}'\cdot\nabla' G \ ,$$
$$=\int (1-k)\left[-\frac{y}{\xi}-\gamma\kappa\right]\hat{\mathbf{n}}'\cdot\nabla' G \ . \tag{10}$$

We will refer to this case as the quasisymmetric model to distinguish it from the symmetric model of Langer and Turski;[5] in that model, k was set equal to 1, after rescaling of the dimensionless parameters to absorb the factor $1-k$ in the right-hand side of Eq. (10).

The other limit is the one-sided model. If we *define* this limit by the condition that $\alpha\hat{\mathbf{n}}\cdot\nabla c_2$ approach zero as $\alpha\to 0$, then we immediately find the result $\phi=-2\hat{n}_y c_S$. Therefore in this limit Eq. (10) becomes

$$0=1+\int c_L\hat{\mathbf{n}}'\cdot\nabla' G_L+\int 2\hat{n}'_y c_S G_L \ . \tag{11}$$

This result can also be obtained directly by only considering the concentration in the liquid region. However, it does not arise as the limit of the general problem as the solid diffusivity is made small. This is because at all $k\neq 0$ the concentration field c_S varies along the interface, and therefore will also vary inside the solid. In fact, for a small diffusion constant, a boundary layer builds up inside the solid; we will see this explicitly in an asymptotic solution for the "cusp" region. Thus this limit does not actually exist unless the concentration inside the solid is constant, which in our model can only occur at $k=0$. The condition $k=0$ was used in an earlier study[14] of growth from solution in a channel geometry. Here, however, the presence of a thermal gradient demands that we assume that there does in fact exist a temperature at which the material can solidify at $c=1$, or in other words $k\neq 0$. Therefore the one-sided model cannot arise from the limit $\alpha\to 0$ of the full problem.

Let us reconsider the derivation of the asymptotic shape of a cell in the "tail" region. For the one-sided model, we can approximate

$$c\approx -\frac{y(x)}{\xi}+\frac{x^2}{\xi}+O\left[\frac{x^4}{y}\right] \tag{12}$$

for large y. Imposing the velocity condition

$$-\frac{\partial c}{\partial x}=-2(1-k)\left[\frac{-y}{\xi}\right]\frac{\partial x}{\partial y}$$

leads to the well-known result

$$(1-k)\frac{dx}{x}=-\frac{dy}{y}$$

or $y\approx y_0 x^{k-1}$. This is the standard result, orginally found by Scheil; for a discussion see Ref. 15. Now let us do the same calculation with a finite solid diffusivity. To a similar level of approximation, the concentration in the solid is

$$c\approx -k\frac{y(x)}{\xi}+k\frac{(p-x)^2}{\alpha\xi}+O\left[\frac{x^4}{y}\right] \ . \tag{13}$$

The Stefan condition [Eq. (6c)] now reduces to the equation

$$x+pk=(k-1)y\frac{\partial x}{\partial y} \ . \tag{14}$$

For x of order pk, the cusp must stop and the interface must remain finite. In other words, there is a lower bound to the cell depth, of order k^{1-k}. For small k, this depth can be quite large, but not infinite. It is interesting to note that using a completely different argument, McFadden *et al.*[9] have derived a bound on cell size for the case $k\geq 1$, a case which have not considered.

The above result regarding cell depth is valid independent of the value of α. In fact, α has completely dropped out of the above analysis since the concentration in the solid develops a boundary layer on the scale α so as to satisfy the equation. Thus it is k that determines how deep the cell can go; the small values of k in actual physical systems is the real reason the one-sided model cusp shape seems to agree with the experimentally observed interface in the tail region.

III. COMPUTATIONAL TECHNIQUE

In this section we formulate a computational procedure for studying solutions of the interface equations derived above. For simplicity, we deal here only with the quasisymmetric model, Eq. (10). This limit is not applicable to most solidification problems[4,16,17] but can be realized by studying liquid-crystal interfaces.[18] This model is sufficient for our purposes since the structure of the steady-state problem seems qualitatively independent of this level of detail once the system is taken far above threshold. A final quantitative comparison with experimental results must of course await study of the full set of equations.

We are interested in constructing solutions which are periodic under $x\to x+\lambda$ and that are symmetric under $x\to -x$. Let us parametrize the interface as follows. We pick points of equal arclength separation running from $i=0$ at the tip to $i=N$ at the half-wavelength point. Then we define a midpoint j to lie between $i=j-1$ and $i=j$; hence j runs from 1 to N in the same interval. Our independent variables will be taken to be $\theta_j\equiv\theta(s_j)$, for interface normal angle $\hat{\mathbf{n}}\cdot\hat{\mathbf{y}}=\cos\theta$. Hence there are N such variables. The positions x_i and y_i are then fixed by the formulas

$$x_i=x_{i-1}+ds\cos\theta_i \ ,$$
$$y_i=y_{i-1}-ds\sin\theta_i \ . \tag{15}$$

By assumption $x_0=0$ and ds is fixed by the requirement that $x_N=\lambda/2$. Finally, y_0 is an extra independent variable that needs to be found as part of the solution.

We now need $N+1$ equations. The first step is to impose the integral equation at the points $i=1,2,\ldots,N-1$; that is, everywhere excluding the in-

terval endpoints. We will shortly describe how to do this. The last two equations arise from the requirement that a physical solution has vanishing slope at both the tip and at the symmetry point (tail). This gives rise to the second-order accurate conditions $\theta(s=0)\approx\frac{3}{2}\theta_1-\frac{1}{2}\theta_2=0$ and $\theta(s=s_{\rm tot})\approx\frac{3}{2}\theta_N-\frac{1}{2}\theta_{N-1}=0$. It is sometimes convenient to temporarily suspend either one or both of these conditions, replacing it by a constraint on, say, the value of y_0. This allows us to search through the space of different interfaces for multiple steady states coexisting at the same parameter values. We will see how this works in Sec. IV.

The integral in the evolution equation can be evaluated by the trapezoidal rule after handling two subtleties. First, there is an extra δ-function contribution at the point $s=s'$ of magnitude $\frac{1}{2}(1-k)(y/\xi+\gamma\kappa)$ which must be added explicitly. Second, $\partial G/\partial y'$ contains a logarithmic divergent piece which must be explicitly subtracted out. To do this, we replace

$$\hat{n}'_y\frac{\partial G}{\partial y'}\left[\frac{y'}{\xi}+\gamma\kappa'\right]$$

with

$$\hat{n}'_y\frac{\partial G}{\partial y'}\left[\frac{y'}{\xi}+\gamma\kappa'\right]+\frac{\hat{n}_y}{4\pi}\left[\frac{y}{\xi}+\gamma\kappa\right]\ln(s-s')^2\ , \tag{16}$$

which has a finite limit as $s\to s'$. The last term can be integrated analytically since none of the factors depend on s' and the resulting expression can be added back in. Once this is done, the integral is given correctly to $O(1/N^2)$ by the trapezoidal rule.

The last issue to be discussed is our evaluation of the infinite sum in the diffusive Green's function. As is easy to show, the sume can be performed analytically in the limit of small p, reproducing the periodic Laplacian Green's function. We make use of the result to rewrite G as

$$G=\frac{1}{4p}e^{-(y-y'+|y-y'|)}-\frac{e^{-(y-y')}}{4\pi}\ln\left[1+e^{-2\pi|y-y'|/p}-2\cos\left[\frac{\pi(x-x')}{p}\right]e^{-\pi|y-y'|/p}\right]$$
$$+\frac{e^{-(y-y')}}{2p}\sum_{m=1}^{\infty}\cos\left[\frac{m\pi(x-x')}{p}\right]\left[\frac{e^{-k_y|y-y'|}}{k_y}-\frac{e^{-k_x|y-y'|}}{k_x}\right], \tag{17}$$

where $k_x=m\pi/p$ and $k_y=(1+k_x^2)^{1/2}$. The last sum converges at least as fast as $1/m^2$ for arbitrary values of $|y-y'|$.

A similar analysis must be done for $\hat{\mathbf{n}}'\cdot\nabla' G$. Considering the derivative of the above sum, one term is of the form

$$\frac{e^{-(y-y')}}{2p}\left[\hat{n}'_x\sum_{m=1}^{\infty}k_x\sin\left[\frac{m\pi(x-x')}{p}\right]\left[\frac{e^{-k_y|y-y'|}}{k_y}-\frac{e^{-k_x|y-y'|}}{k_x}\right]\right.$$
$$\left.+\operatorname{sgn}(y-y')\hat{n}'_y\sum_{m=1}^{\infty}\cos\left[\frac{m\pi(x-x')}{p}\right](e^{-k_y|y-y'|}-e^{-k_x|y-y'|})\right].$$

These last two sums do not converge sufficiently well, and we therefore need to use another subtraction. We replace these expressions with

$$\frac{e^{-(y-y')}}{2p}\left\{\sum_{m=1}^{\infty}\hat{n}'_x\sin\left[\frac{m\pi(x-x')}{p}\right]\left[\frac{k_x}{k_y}e^{-k_y|y-y'|}-e^{-k_x|y-y'|}\left[1+\frac{A}{k_x}\right]\right]\right.$$
$$\left.+\operatorname{sgn}(y-y')\sum_{m=1}^{\infty}\hat{n}'_y\cos\left[\frac{m\pi(x-x')}{p}\right]\left[e^{-k_y|y-y'|}-e^{-k_x|y-y'|}\left[1+\frac{A}{k_x}\right]\right]\right\} \tag{18}$$

with $A=p|y-y'|/2$. This replacement then requires us to add to $\hat{\mathbf{n}}'\cdot\nabla G$ the extra term

$$\frac{Ae^{-(y-y')}}{2\pi p}\left[\hat{n}'_x\tan^{-1}\frac{e^{-\pi|y-y'|/p}\sin\left[\frac{\pi(x-x')}{p}\right]}{1-e^{-\pi|y-y'|/p}\cos\left[\frac{\pi(x-x')}{p}\right]}\right.$$
$$\left.+\hat{n}'_y\operatorname{sgn}(y-y')\ln\left[1+e^{-2\pi|y-y'|/p}-2\cos\left[\frac{\pi(x-x')}{p}\right]e^{-\pi|y-y'|/p}\right]\right]. \tag{19}$$

This completes the derivation of a tractable expression for the required Green's functions.

In a recent paper,[10] Karma suggested that a useful simplification of G occurs if one just drops the last term in Eq. (17). This incurs a uniform error of $(p/\pi)^2$ which is typically small. A similarly useful approximation for the normal derivative can be obtained by dropping the final sum of Eq. (18), keeping the additional contribution given above. We will use this approximate expression in much of this work, occasionally checking that this truncation makes no qualitative difference in the results.

The resulting set of nonlinear equations is then iterated by using Newton's algorithm. We either start from planar interfaces with fixed amplitude constraints or from initial guesses based on solutions in nearby regions of parameter space. The actual program used was the MINPACK routine HYBRD, with the iteration ended upon reaching a relative accuracy of 10^{-5}. In practice, if there is a solution for the set of parameters being tested the algorithm converges quite rapidly and any desired accuracy can be easily achieved.

The parameter space for this problem is quite large and therefore impossible to study exhaustively. Instead, we fix several parameters, roughly in accord with the values measured by de Cheveigne *et al.*[16] in a CBr_4 experiment, using Br_2 as the impurity. In particular, we use throughout $k=0.16$ and $l_T=1.21\times10^{-2}v$ (μm/sec). The physical value of the anisotropy is probably about 10–20% (15 times the measured anisotropy in the radius of an equilibrium bubble), although it has not been accurately measured. As already mentioned, we will use a quasisymmetric model although the physical diffusivity ratio α is probably around 0.1. Finally, the measured value of γ is $0.89\times10^{-4}v$ (μm/sec), but instead we chose a larger value of $9.95\times10^{-4}v$ (μm/sec) for computational simplicity (see below).

Near threshold, we find that 25 points are sufficient to find accurate solutions at the chosen value of γ. Clearly, as we increase the driving velocity, the number of points needed to resolve the structure increases. At the final stage of our current calculations, $v\approx8v_{\rm crit}$, 100 points suffice. Had we used the physical value of γ even more would have been necessary. Since our aim is to study generic behavior, we increased the surface energy as discussed above so as to cut down on our computer time requirements. Since the time requirement of Newton's algorithm scales as N^3, this represents a considerable savings.

IV. RESULTS NEAR THRESHOLD

In this section we present the results of our study of steady-state solutions near the threshold for the Mullins-Sekerka instability of the planar interface. This study was carried out with the purpose of verifying the picture that has emerged from the analytical bifurcation theory as well as the computational studies of Ungar and Brown.[7] Afterwards, we proceed to study the highly nonlinear regime encountered at larger velocities.

A planar interface solution for this system exists with $y=-l_T/k$. This solution undergoes a morphological instability as v is increased. In Fig. 4 we show the neutral stability curve for the parameters chosen in Sec. III:

$$\omega=2\tilde{Q}+\frac{k}{k-1}(\gamma q^2+l_T^{-1})[k\tilde{Q}+Q+2(k-1)] \quad (20)$$

with wavelength $\lambda=2\pi/q$ and

$$Q=1+(1+\omega+q^2)^{1/2}\ ,$$

$$\tilde{Q}=-1+(1+\omega+q^2)^{1/2}\ .$$

(Notice that the wavelength is scaled with the diffusion length.) The neutral curve is quite wide at the bottom and we therefore might expect mixing of the initially unstable wave vector with its harmonics to occur rapidly as we move beyond threshold.

There have been several analytical studies[5] of the weakly nonlinear problem slightly above onset. The most general of these works are those of a Caroli, Caroli, and Roulet (CCR) and Wolkind, Oulton, and Sriranganathan which can be immediately adapted to the case at hand. (These works disagree by a factor that in our case does not alter the nature of the bifurcation.) Using the formulas from Caroli *et al.* with the identification (CCR on the left)

$$a_0=\omega/4\ ,$$

$$\omega=q/2\ ,$$

$$\beta/2=-\frac{k}{k-1}\gamma\ ,$$

$$\tau=1+\frac{k}{(k-1)}\frac{1}{2l_T}\ ,$$

and the limits $\eta=n=1$, we can directly carry over their calculation of the third-order coefficient in the amplitude equation

$$\frac{dy}{dt}=\omega y-a_1y^3\ . \quad (21)$$

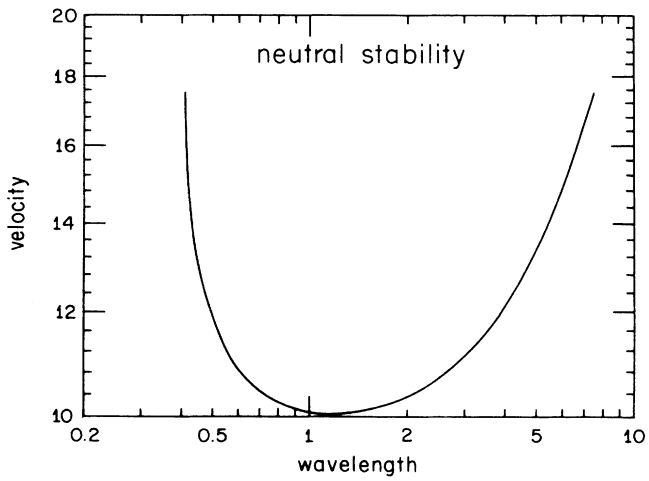

FIG. 4. Neutral stability curve for the quasisymmetric model.

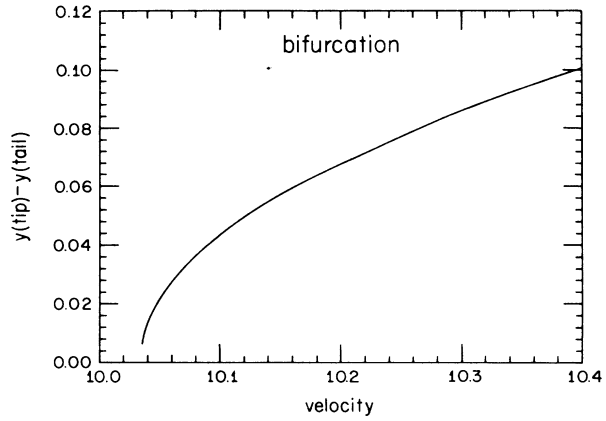

FIG. 5. Amplitude vs velocity near onset.

The result is that a_1 is positive, indicating a supercritical bifurcation. In Fig. 5 we have plotted twice the amplitude (in diffusion length units) versus v, verifying this result. For comparison, setting $\alpha=0$ gives rise to a_1 negative, in accord with the more usual behavior of realistic solidification systems.

Let us now set $\epsilon=0$, $\lambda=1.2$ and look for solutions, using $N=50$ and the simplified Green's function. To this end, we relax the boundary condition at the tip and instead fix y_0. In Fig. 6 we have plotted y_0' versus y_0 at $v=12$ μm/sec, showing that there are three roots. The root as largest y_0 is a direct continuation of the solution which bifurcated from zero at the threshold for this wavelength. This solution is shown in Fig. 7(a) as a function of the velocity. This curve is generated by starting with the actual solution at $v=12$ μm/sec and slowly decreasing v while maintaining the condition $y_0'=0$. The third branch is a solution which is actually periodic in one half of the cell, i.e., actually has wavelength $\lambda/2$; it starts from the bifurcation for the $\lambda=0.6$ mode which can be shown to occur at $v\sim 10.5$ μm/sec. This behavior is shown in Fig. 7(b).

Finally, the intermediate branch is shown in Fig. 7(c); as v decreases it goes from a mode of wavelength λ to one of wavelength $\lambda/2$, which is in fact identical with the third branch. Most importantly, as we pass $v\approx 12.1$ μm/sec this branch merges with and annihilates the upper branch. This seems to occur roughly where the tip curvature goes to zero from above on the upper branch and below, on the second branch. A schematic picture of this behavior is shown in Fig. 8. This means that for velocities past a critical one (around 12.1) there exist no solutions at the primary unstable wavelength.

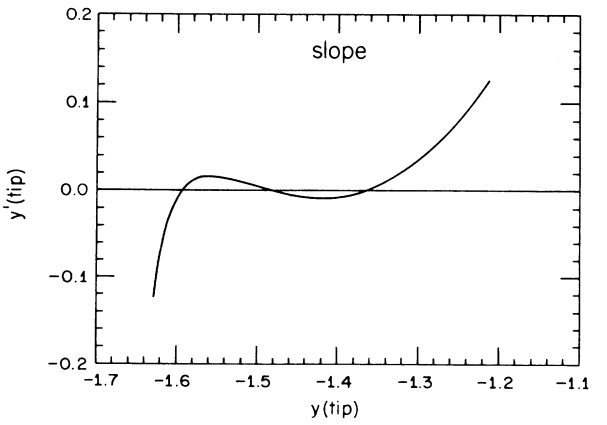

FIG. 6. Mismatch condition for finding multiple steady-state solutions.

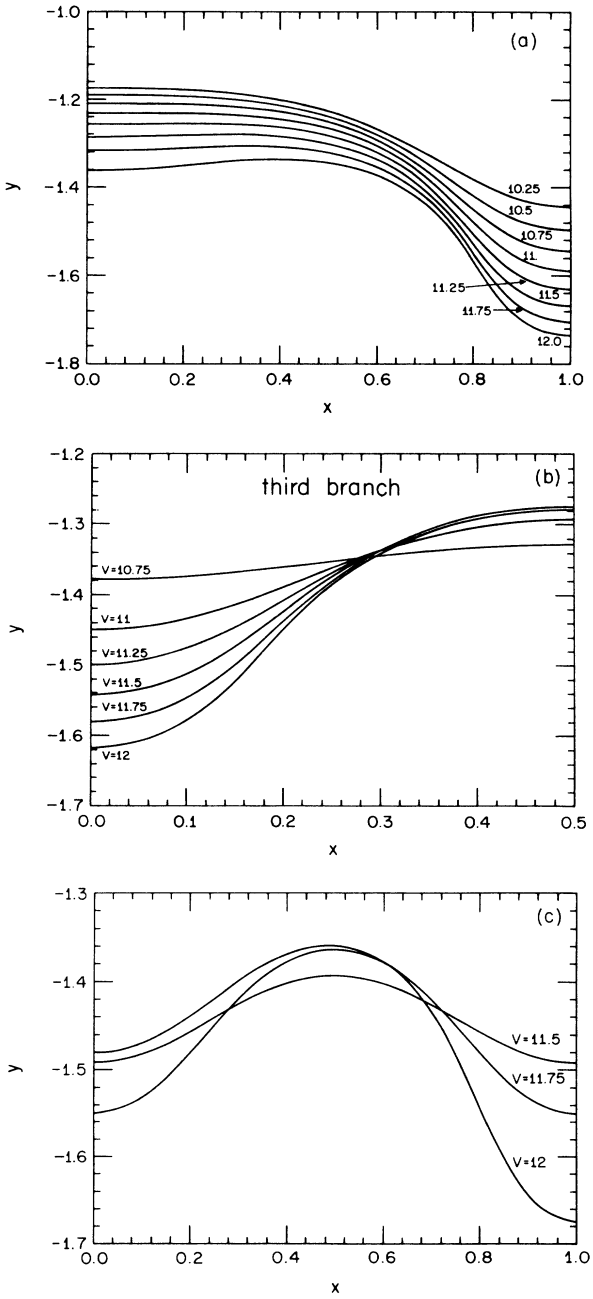

FIG. 7. Solution branches for $10\le v\le 12$ in units of μm/sec. (a) Main branch, (b) $\lambda/2$ branch, and (c) mixed branch.

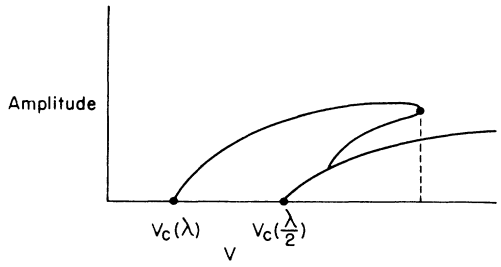

FIG. 8. Bifurcation diagram showing fold and symmetry breaking bifurcation.

This type of behavior is identical to that discussed by Langer and Turski, based on a two mode truncation and by Ungar and Brown. It occurs both in the supercritical case discussed here and in the subcritical case of the actual metallurgical systems. The most general treatment of this type of bifurcation diagram seems to be the work of Dangelmayer[19] on steady-state bifurcations in the presence of an O(2) symmetry, translations, and reflections. In his language, the intermediate solution is a mixed mode that emerges from the pure $\lambda/2$ solution branch in a symmetry breaking secondary bifurcation.

The branch at $\lambda=0.6$ can be extended to higher velocities. In Fig. 9(a) we show the slow variation of the pattern as v is increased to 20, which is about two times threshold. The cells become deeper but otherwise do not change significantly. One interesting feature is the liquid "bubble" near the tail region, which we can see more clearly when we draw the x-y axes on a common scale, as in Fig. 9(b). This again verifies a similar finding by Ungar and Brown for deep cells.

At $v=30$ μm/sec we can investigate the effect of varying λ; this is in some sense the reverse of our earlier strategy. In Fig. 10(a) we plot the solution versus λ, in units of the initial half wavelength (0.3). The branch ends at $\lambda\approx 2.5$ in much the same way as discussed earlier; there is a second branch, plotted in Fig. 10(b), which merges with and annihilates the main one. As we go "around the bend," this second solution becomes a $\lambda/2$ mode. What is happening is clear. The tip curvature on the main branch is decreasing, eventually reaching zero near the bend. It then continues to decrease, causing the tip to become a local minimum which deepens as we go further. Eventually the local minimum at the tip becomes identical to the minimum at the cell edge, and the wavelength

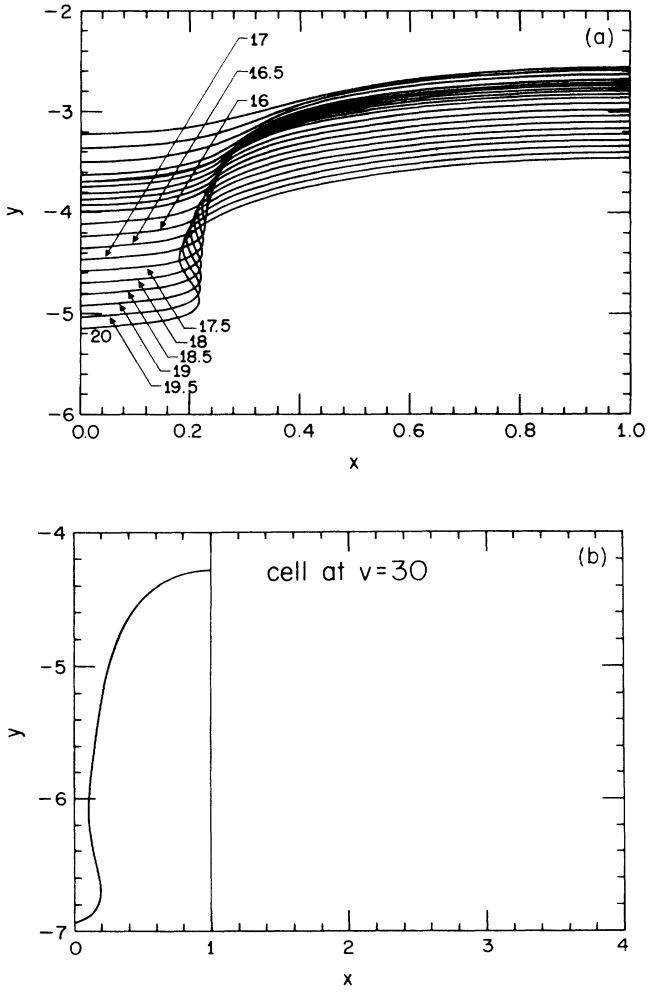

FIG. 9. (a) Cell shape vs velocity at $\lambda=0.6$. (b) $v=30$ μm/sec drawn to scale.

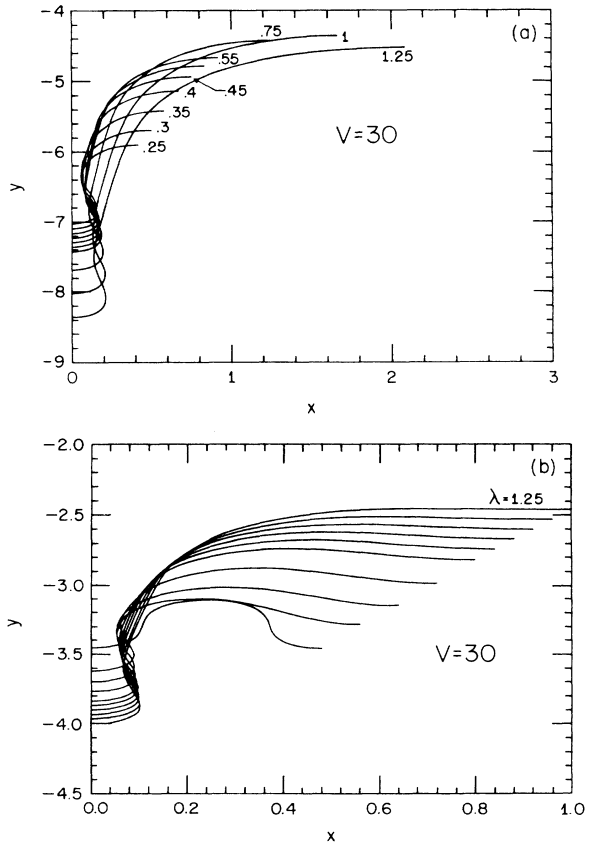

FIG. 10. The "bend" near $\lambda=2.5$. (a) Main branch, (b) mixed branch vs λ.

has halved. There are no other branches, and so there are in fact no steady-state solutions for $v=30$ μm/sec past a specific wavelength. This maximum wavelength is in general much smaller than one would guess by simply looking at the curve of neutral stability. There is also a minimum value of λ, since we eventually approach the neutral curve in the other direction.

Other points worth noting include the following.

(1) There is very little dependence on anisotropy in this range. We have studied $\epsilon=0.1$ in addition to $\epsilon=0$ with no discernible qualitative change.

(2) We have occasionally used the full Green's function (truncated to enough terms for relative accuracy of 0.01%), again with no qualitative change to the quoted results.

(3) The behavior of the solution branch in this reason seems to be qualitatively the same as that found by Ungar and Brown[7] in their model which had a subcritical bifurcation. We therefore will continue to assume that our quasisymmetric system does not miss any important aspect of the physics of these steady-state solutions once one is reasonably far above threshold.

V. THE HIGHLY NONLINEAR REGIME

As we increase the driving velocity, we reach a regime that has yet to be studied by either computational or analytical methods. We are particularly interested in two issues. In the experiment of de Cheveigne *et al.*, upon which our analysis is loosely based, the actual wavelength was observed to vary as $v^{-1/2}$. This appears to be a fairly universal finding in studies of directional solidification. We would like to see if any possible explanation of this can emerge from our considerations here. First, however, we would like to elucidate the connection between the solvability mechanism derived for other solidification systems and the tip selection problem here. To do this, it is beneficial to consider what happens to our steady-state solutions as the surface tension is taken very small.

In Fig. 11 we show the shape at $v=80$ μm/sec, $\lambda=0.6$. Notice the very small bubble caused by the surface tension. In Fig. 12 we show the results of varying the surface tension γ from its large value to the range of values actually relevant for the CBr_4 system. The important fact to note is that there exists an intermediate asymptotic regime in which the shape is independent of γ. Eventually, at small enough x we reach the bubble which is highly sensitive to surface energy, and the "universal" curve breaks down. Presumably, a boundary layer method of analysis could capture the behavior in this region. We can contrast this to the way in which the tip region depends on γ. The tip seems to be going smoothly to a particular limiting shape, in a way which is similar to the behavior of the tip of a viscous fluid finger for small surface energy.[20]

The intermediate asymptotic behavior is in agreement with the cusp region solution given in Sec. II, which also did not depend on γ. This feature shows that it is possible, in some sense, to define a tip region problem which matches onto the universal curve and thereby drop the necessity of solving for the interface all the way down to the bubble. This tip region problem, then, is characterized by trying to find a tip shape consistent with a given velocity; it is quite similar to the familiar problems of a free dendrite or a viscous finger where we impose the asymptotic shape and the velocity, and ask for the tip curvature. So, the directional solidification problem at *fixed* wavelength can be thought of as a selection problem of the same general class as those shown to be analyzable in terms of a surface tension induced solvability condition. This shows most clearly, though, that the solvability mechanism cannot determine the spatial wavelength of the pattern. Our results agree completely with those of Dombre and Hakim, and Ben-Amar and Moussallam in this regard.

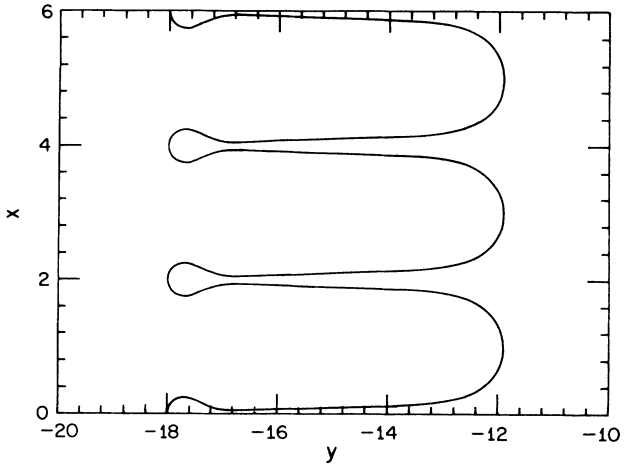

FIG. 11. Deep cell shape at $v=80$ μm/sec.

It is worthwhile to expand a bit on this last point. Thinking of the tip shape selection as an example of the microscopic solvability mechanism[3] allows us to make several immediate predictions. First, we expect that at any finite γ, there is not one but a discrete set of possible tip shapes; one and only one of these shapes is expected

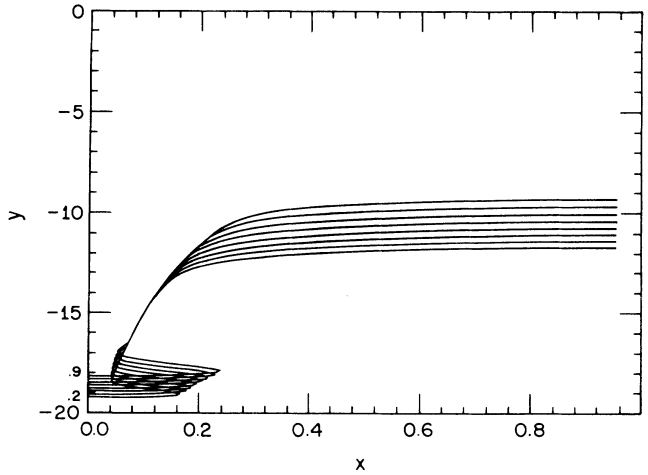

FIG. 12. Dependence of shape on surface energy γ.

to be linearly stable with respect to tip deforming perturbations. As $\gamma \to 0$, this discrete set converges to one solution; at $\gamma = 0$ exactly, though, a continuous set is possible. If we relax the condition that $y'(0)=0$ as in the solution search of Sec. IV, we expect that the slope will go to zero with an essential singularity as a function of γ, for all tip shapes (and positions) that are part of the continuum. Note that this predicted continuum at fixed wavelength precisely corresponds to the double continuum of Ben-Amar and Moussallam.

Why should there be a continuum of possible tip shapes [and related positions $y(0)$] at $\gamma = 0$? Let us first fix $y(0)$ and allow nonzero values of $y'(0)$. A nonzero value of this slope would mean that there is a cusp in the interface near $y(0)$. The concentration field near this cusp would be singular, with the local structure $c \sim r^{\alpha}$, where $\alpha = \pi/\phi$ for opening angle $\phi = \pi - y'(0)$. The curvature term could match this singularity in the equations with a judicious choice of the interface near this point; this, however, requires $\gamma \neq 0$. Thus a purely local analysis allows a cusp in the presence of surface tension and a new equation must therefore require that the cusp magnitude vanishes; for zero surface tension, the cusp magnitude vanishes identically, removing one equation and hence allowing us to arbitrarily fix $y(0)$, at least over some range.

We have been able to verify at least some aspects of this picture. There are several solutions at $v = 80\ \mu$m/sec; furthermore the solutions corresponding to secondary branches have a more complex tip structure than that of the main branch shown in Fig. 11. This is exactly the same as what happens for the other known examples of the solvability mechanism. The solutions move closer as γ is lowered, and seem to asymptotically approach $y(0) = -8.3$. This solution appears to be analogous to $\lambda = \frac{1}{2}$ for the Saffman-Taylor finger.[20] Finally, the value of $y'(0)$ at this tip position seems to monotonically go to zero with a form that is at least qualitatively consistent with an exponentially singular form. So far, everything we have done indicates that the solvability analysis is likely to be valid for this system.

Let us now focus on the λ and ϵ dependence of our results. The anisotropy again plays no crucial role; this must change eventually since we known that anisotropy becomes important as the shape becomes more like a parabolic dendrite, but no sign of this has appeared at this velocity. As λ changes, though, there is still a "bend" (or fold) at some $\lambda_{\max}$ past which no solutions exist. The dependence of the maximum λ is plotted versus $\sqrt{v}$ in Fig. 13 for the cases of $\epsilon = 0$, 0.1. Notice that the results are almost exactly straight lines. That is, the band edge obeys the scaling $\lambda_{\max} \sim \sqrt{v}$. But if we recall that we have scaled all our lengths by the diffusion length $v/2D_L$, we see that the wavelength in physical units will scale as $v^{-1/2}$. This happens to agree with the experimental measurement.

Why might the band edge have something to do with wavelength selection?[21] First, we have already mentioned that a similar structure has emerged in a recent study of Taylor-Couette flow.[13] As already discussed, this type of fold is a generic effect in systems with strong coupling between modes at λ and $\lambda/2$. The occurrence of the fold is always connected to the appearance of a new structure "in between" the previous peaks of amplitude; here this happens via the tip becoming a local minimum, in Taylor-Couette flow, via the formation of an additional vortex.

The next point to note is that there is some indication that the Eckhaus stability boundary lies close to the fold. This was seen explicitly in Taylor-Couette flow,[13] and let us assume that the same happens here. Then, slowly increasing v will temporarily leave the system with too large a wavelength when p crosses $p_{\max}$. The system will then tip split and thereby create new cells until it manages to get to the other side of the fold. This scenario assumes that (a) tip splitting is dynamically possible and (b) there is no tendency to drift once the stable state is reached. The former argument seems valid in materials like succinonitrile[4] and carbon tetrabromide,[16] but is defintely not true for strongly anisotropic crystals such as pivalic acid.[17] The second point is harder to verify without a complete dynamical theory. There have been some suggestions[22] that there will still be tendency to drift towards a final wavelength under the effects of noise, and this certainly bears further investigation. Note that if anything like the above idea is correct, there might be a measurable hysterisis in wavelength versus velocity.

We do not yet understand why our numerical calculations gave rise to the behavior $\lambda \sim \sqrt{v}$. It is worth noting though, that this is equivalent to stating that the important control parameters for the wavelength problem are

$$\gamma' \equiv \gamma/p^2, \quad l_T' = l_T/p^2 .$$

These rescaled dimensionless variables are exactly what one would recover if one took the "Saffman-Taylor" limit ($p \to 0$) of the problem at hand. This is the reason Karma[23] found $\lambda \sim v^{-1/2}$ in his study of the channel problem with unit undercooling. Why the scaling associated with this limit should be relevant near Peclet numbers of order 1 is not clear, although the correct parameter may be

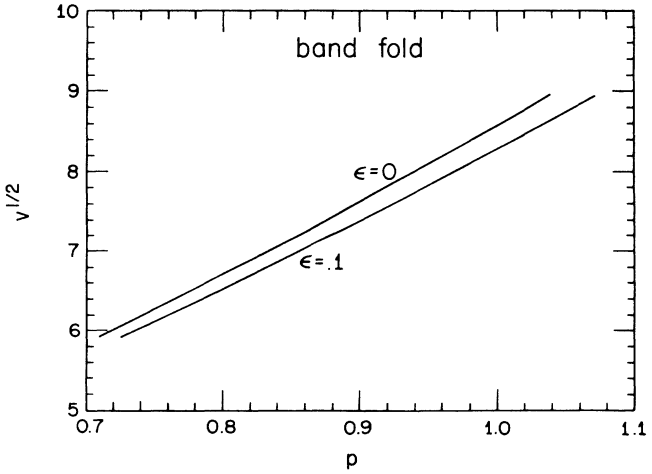

FIG. 13. Bend location vs velocity at two different anisotropies.

p/π. This is consistent though with the aforementioned comments regarding anisotropy and the fact that the shapes are closer to neighboring fingers than to neighboring parabolic dendrites.

VI. OUTLOOK

We have presented a straightforward but extremely powerful scheme for solving the steady-state problem in directional solidification. We have reproduced the picture of Langer and Turski, and Ungar and Brown, for states close to the onset of the Mullins-Sekerka instability. Also, we have shown how the $\lambda \rightarrow \lambda/2$ bifurcation may be important for wavelength selection. It is still too early to be sure, but we feel that the boundary integral approach will prove to be the method of choice for the problem of steady-state cellular solidification. Of course, it may still be necessary to use the finite-element approach for the study of time-dependent processes.

There are several tasks that need to be undertaken. First, we would like to focus on the particular experimental setup of de Cheveigne and study a fully realistic model. Next, we must augment the steady-state calculations with linear stability analyses, including the possibility of Bloch-like modes on the underlying periodic system. This should lead to the usual Eckhaus boundary near threshold which then could be extended to higher v. As discussed previously, it is important to know if the stability edge is close to the band fold, as has been seen in Taylor-Couette studies.

An important part of our results concerns the suggestion that microscopic solvability works so as to determine tip shape and position, for fixed wavelength. A very interesting question arises as to whether anything similar could be seen in other pattern-forming systems that form periodic patterns, specifically, we can ask whether there is any singular behavior in, say, Taylor-Couette patterns, if we fix the wavelength and take the viscosity to zero. We are currently investigating this issue.

A final issue yet to be addressed is the transition to dendritic growth. We expect that this transition is noise driven,[24,25] requiring a finite amplitude excitation to move the system away from the linearly stable cell shape. For a fixed amount of noise, sidebranching will set in at differing velocities, depending on parameters such as the crystalline anisotropy. Given the steady-state solutions found here, it should be possible to investigate this issue by numerical computations.

There have been many ideas put forth regarding wavelength selection in systems with an allowed band of steady-state patterns. It turns out that there is no unique answer to this problem; different experimental protocols can and do lead to different wavelengths. The methods given here plus the extensions just mentioned should allow us to decide if a particular dynamical selection mechanism is operating in a particular experiment. This can be done by making quantitative predictions for experimentally observable shapes. Coupled with similar progress toward analyzing steady-state eutectic growth,[26] this study should eventually lead to the development of a systematic procedure for computing solidification microstructure in the cellular regime.

Note added. After completion of this manuscript, we were made aware of a recent work by Ramprasad, Bennett, and Brown, using the finite-element method for deep finite cells.[27] This work also studies the issue of wavelength bands for deep cells and comes to exactly the same conclusions as those contained herein. This paper does not deal with the relationship between deep cells and the infinite cells in the one-sided limit as studied by Karma, Dombre, and Hakim and by Ben-Amar and Moussallam, nor does it deal with the relevance of the solvability mechanism (as discovered for free dendritic growth) for the tip shape of the cellular structure.

ACKNOWLEDGMENTS

The work of one of us (D.A.K.) was supported by U.S. Department of Energy Grant No. DE-FG-02-85ER54189. H.L. was supported in part by a grant from the U.S. Defense Advanced Research Projects Administration under University Research Initiative, Grant No. N00014-86-K-0758.

[1]J. S. Langer, Rev. Mod. Phys. **52**, 1 (1980); D. P. Woodruff, *The Solid-Liquid Interface* (Cambridge University Press, Cambridge, England, 1973).

[2]M. E. Glicksman Mater. Sci. Eng. **65**, 45 (1984); A. Dougherty and J. P. Gollub (unpublished).

[3]For recent reviews, see D. Kessler, J. Koplik, and H. Levine, Adv. Phys. **37**, 255 (1988); J. Langer, in *Chance and Matter*, edited by J. Souletie *et al.* (North-Holland, Amsterdam, 1987).

[4]K. Somboonsuk, J. T. Mason, and R. Trivedi, Metall. Trans. **15A**, 967 (1984).

[5]D. J. Wollkind and L. A. Segel, Philos. Trans. R. Soc. London **268**, 351 (1970); J. S. Langer and L. A. Turski, Acta Metall. **25**, 1113 (1977); B. Caroli, C. Caroli, and B. Roulet, J. Phys. (Paris) **43**, 1767 (1982); D. J. Wollkind, D. B. Oulton, and R. Sriranganathan, *ibid.* **45**, 505 (1984).

[6]W. W. Mullins and R. F. Sekerka, J. Appl. Phys. **34**, 323 (1963); **35**, 444 (1964).

[7]L. H. Ungar and R. A. Brown, Phys. Rev. B **29**, 1367 (1984); **30**, 3993 (1984); **31**, 5923 (1985); **31**, 5931 (1985).

[8]G. B. McFadden and S. R. Coriell, Physica D **12**, 253 (1984).

[9]For the most recent applications of the methods developed in Refs. 7 and 8, see G. B. McFadden, R. F. Boisvert, and S. R. Coriell, J. Cryst. Growth **84**, 371 (1987); J. D. Hunt and D. G. McCartney, Acta Metall. **35**, 89 (1987).

[10]A. Karma, Phys. Rev. Lett. **57**, 858 (1986).

[11]T. Dombre and V. Hakim, Phys. Rev. A **36**, 2811 (1987).

[12]M. Ben-Amar and B. Moussallam, Phys. Rev. Lett. **60**, 317 (1988).

[13]H. Riecke and H.-G. Papp, Phys. Rev. A **33**, 547 (1987), and references therein to earlier work on the Taylor-Couette system.

[14]D. A. Kessler, J. Koplik, and H. Levine, Phys. Rev. A **34**, 4980 (1986).

[15]J. D. Hunt in *Solidification and Casting of Metals* (The Metals Society, London, 1979).
[16]S. de Cheveigne, C. Guthmann, and M. M. Leburn, J. Phys. (Paris) **47**, 2095 (1986).
[17]J. Bechhoefer and A. Libchaber, Phys. Rev. B **35**, 1393 (1986).
[18]P. Oswald, J. Bechhoefer, and A. Libchaber, Phys. Rev. Lett. **58**, 2318 (1987).
[19]D. Dangelmayer, Dyn. Stability Syst. **1**, 159 (1986). For the application of this approach to directional solidification, see P. Haug, Phys. Rev. A **35**, 2733 (1985).
[20]J. M. Vanden-Broeck, Phys. Fluids **26**, 2033 (1983); D. A. Kessler and H. Levine, Phys. Rev. A **33**, 2621 (1986); **33**, 2634 (1986); D. C. Hong and J. S. Langer, Phys. Rev. Lett. **56**, 2032 (1986); B. I. Shraiman, *ibid.* **56**, 2028 (1986).
[21]This idea was suggested by H. Riecke (private communication).
[22]M. Kerszberg, Phys. Rev. B **27**, 3909 (1983); **27**, 6796 (1983); **12**, 262 (1984).
[23]A. Karma, Phys. Rev. A **34**, 4353 (1986).
[24]R. Pieters and J. S. Langer, Phys. Rev. Lett. **56**, 1948 (1986).
[25]D. Kessler and H. Levine, Europhys. Lett. **4**, 215 (1987); M. Barber, A. Barbieri, and J. S. Langer, Phys. Rev. A **36**, 3340 (1987); B. Caroli, C. Caroli, and B. Roulet, J. Phys. (Paris) **48**, 1423 (1987).
[26]D. Kessler and H. Levine (unpublished).
[27]A preliminary version of their results appeared in *Supercomputer Research in Chemistry and Chemical Engineering,* edited by K. Jensen and D. Truhlar (American Chemical Society, Washington, D.C., 1987).

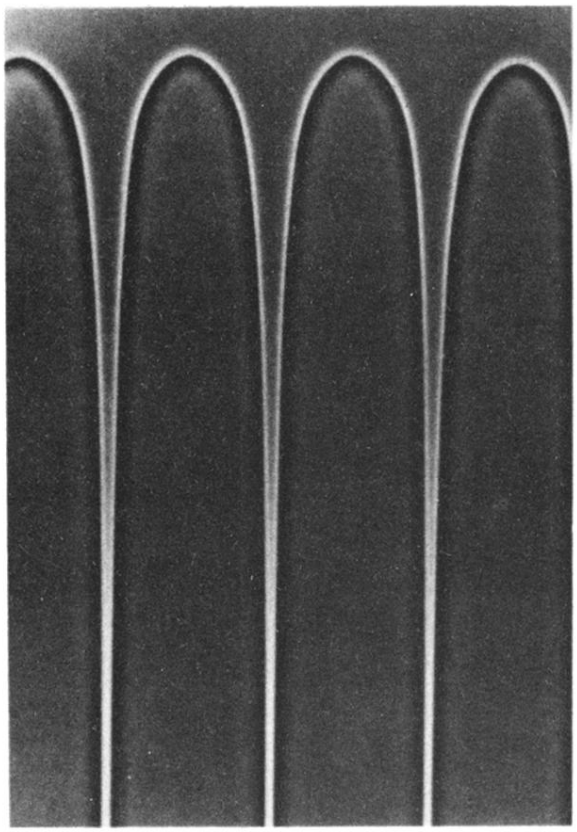

FIG. 1. Typical cellular structure seen in thin-film directional solidification of pivalic acid (see Ref. 17) (courtesy A. Libchaber).